Selecting the Optimal Factor of Safety or Probability of Liquefaction Triggering for Engineering Projects Based on Misprediction Costs

Sneha Upadhyaya, S.M.ASCE[1]; Brett W. Maurer, M.ASCE[2]; Russell A. Green, M.ASCE[3]; and Adrian Rodriguez-Marek, M.ASCE[4]

Abstract: In deterministic evaluations, liquefaction triggering potential is assessed by comparing the computed factor-of-safety (FS) against liquefaction triggering to some minimal acceptable FS. While some guidelines are available for selecting the minimal acceptable FS, there is no standard value. Herein, Receiver Operating Characteristic (ROC) analyses are used to develop an approach for selecting the optimal minimal acceptable FS (i.e., optimal FS) for a project based on the relative costs of mispredictions. Utilizing different liquefaction triggering models and their associated case-history databases, relationships are established between the optimal FS and the ratio of the cost of a false-positive prediction to the cost of a false-negative prediction (i.e., cost ratio, CR). Also, by combining the FS data from different models, a "generic" FS-CR relationship is developed that "averages out" the degree of conservatism inherent to the individual triggering models. Similarly, relationships relating the optimal probability of liquefaction triggering (PL) to CR are developed for the probabilistic variants of the triggering models, as well as a generic PL-CR curve. **DOI: 10.1061/(ASCE)GT.1943-5606.0002511.**

Introduction

The main objective of this paper is to develop an approach for relating the optimal minimal acceptable factor-of-safety against liquefaction triggering (FS) to the cost of mispredicting liquefaction triggering. "Optimal" herein should be understood as "optimal for decision making," such that remedial action is judicious when the computed FS falls below the optimal value. To this end, the proposed relationships can be used to select the optimal minimal acceptable FS (i.e., "optimal" FS) for a project based on the costs of liquefaction risk-mitigation schemes, relative to the costs associated with the consequences of liquefaction. While this paper focuses on FS, the framework proposed herein is also used to relate the optimal probability of liquefaction triggering (PL) to the relative costs of mispredicting liquefaction triggering.

The stress-based "simplified" model is the most widely used approach for predicting liquefaction triggering at a site. This model was originally developed by Whitman (1971), and Seed and Idriss (1971) for the Standard Penetration Test (SPT) and has been subsequently updated for use with other in situ testing methods such as the Cone Penetration Test (CPT) and small-strain shear wave velocity (V_s) (e.g., Robertson and Wride 1998; Cetin et al. 2004, 2018; Moss et al. 2006; Idriss and Boulanger 2008, 2010; Kayen et al. 2013; Boulanger and Idriss 2012, 2014; Green et al. 2019; among others). Moreover, both deterministic and probabilistic variants of the simplified model have been proposed, where the latter explicitly quantifies and accounts for uncertainties in the model and its input parameters. In a deterministic liquefaction triggering model, the normalized cyclic stress ratio (CSR^*), or the seismic demand, and the normalized cyclic resistance ratio ($CRR_{M7.5}$), or liquefaction capacity, are used to compute an FS against liquefaction triggering

$$FS = \frac{CRR_{M7.5}}{CSR^*} \tag{1}$$

where CSR^* has been normalized to an M7.5 event and corrected for effective overburden stress and initial static shear-stress; and $CRR_{M7.5}$ has been normalized to the same conditions as CSR^* and is computed using a semiempirical relationship based on in situ measurements. These measurements include normalized/corrected SPT blow count ($N_{1,60cs}$), CPT tip resistance (q_{c1Ncs}), and V_s (V_{s1}). Liquefaction is predicted to trigger when $FS \leq 1$ (i.e., when the demand equals or exceeds the capacity).

Using probabilistic variants of these models, PL is generally computed as a function of the predictor variables that correlate to the capacity of the soil (e.g., $N_{1,60cs}$; q_{c1Ncs}; or V_{s1}), the demand imposed by shaking (e.g., CSR^*), as well as the uncertainties in the triggering model. For reasons that will not be discussed here, deterministic $CRR_{M7.5}$ curves often correspond to $PL \approx 15\%$ (e.g., Cetin et al. 2004; Moss et al. 2006; Boulanger and Idriss 2014). Although probabilistic liquefaction triggering models are central to performance-based engineering frameworks, the deterministic model (i.e., FS) still represents the current standard-of-practice for predicting liquefaction triggering. Although in theory, liquefaction should not trigger for $FS > 1$, FS ranging from 1 to 1.5 are generally used as the minimum acceptable value (or as a decision threshold) for design, typically based on "rules of thumb." While such rules of thumb are generally guided by factors such as

[1]Graduate Student, Dept. of Civil and Environmental Engineering, Virginia Tech, Blacksburg, VA 24061. Email: usneha@vt.edu

[2]Assistant Professor, Dept. of Civil and Environmental Engineering, Univ. of Washington, Seattle, WA 98195. Email: bwmaurer@uw.edu

[3]Professor, Dept. of Civil and Environmental Engineering, Virginia Tech, Blacksburg, VA 24061 (corresponding author). ORCID: https://orcid.org/0000-0002-5648-2331. Email: rugreen@vt.edu

[4]Professor, Dept. of Civil and Environmental Engineering, Virginia Tech, Blacksburg, VA 24061. ORCID: https://orcid.org/0000-0002-8384-4721. Email: adrianrm@vt.edu

Note. This manuscript was submitted on March 30, 2020; approved on January 8, 2021; published online on March 17, 2021. Discussion period open until August 17, 2021; separate discussions must be submitted for individual papers. This paper is part of the ***Journal of Geotechnical and Geoenvironmental Engineering***, © ASCE, ISSN 1090-0241.

Table 1. Factors of safety (FS) for liquefaction hazard assessment

Consequences of liquefaction	$N_{1,60cs}$	FS
Settlement	≤15	1.1
	≥30	1.0
Surface manifestation	≤15	1.2
	≥30	1.0
Lateral spreading	≤15	1.3
	≥30	1.0

Source: Data from Martin and Lew (1999).

the uncertainty in the triggering evaluation process, importance of the structure, and consequences of liquefaction, they have been based largely on heuristic approaches. Due to the lack of a standardized method for selecting FS, various guidelines have been proposed in the literature. For example, according to the 2009 NEHRP recommended seismic provisions by the Building Seismic Safety Council (BSSC 2009), FS of 1.1–1.3 is "usually appropriate" for building sites. The use of $FS > 1$ is to account for the chance that liquefaction occurred at depth at some "no liquefaction" case-history sites used to develop the triggering models, but no surficial liquefaction manifestations resulted (e.g., Green et al. 2018). Moreover, they refer to Martin and Lew (1999) (e.g., Table 1) for additional guidance on selecting FS, which considers different ground failure mechanisms (i.e., "settlement," "surface manifestation," and "lateral spreading"), as well as the postliquefaction strain potential of soils having an associated penetration resistance (e.g., $N_{1,60cs}$).

In any engineering project, the choice of the minimal acceptable FS (i.e., the desired degree of conservatism) should account for the consequences, or costs, of mispredicting liquefaction. However, existing guidelines for selecting the minimal acceptable FS do not explicitly account for such misprediction costs. These include the costs of false-negative predictions (i.e., liquefaction occurs, but was not predicted in the design event), which are the costs associated with liquefaction-induced damage (e.g., property damage, reconstruction and rehabilitation costs, etc.); and the costs of false-positive predictions (i.e., liquefaction is predicted, but did not occur in the design event), which could be those associated with the unnecessary or overdesigned liquefaction risk-mitigation schemes (e.g., ground improvement, stronger foundation design and construction, etc.). Clearly, these costs can vary among different engineering projects. For example, the costs associated with mispredicting liquefaction beneath a one-story residential building will be likely very different than those for a similar misprediction beneath a large earthen dam. As such, the optimal FS for a project should be selected based on the associated costs of mispredicting liquefaction triggering.

Accordingly, this paper uses a quantitative, standardized approach to select the optimal FS for a project, based on the costs of mispredicting liquefaction triggering. Toward this end, Receiver Operating Characteristic (ROC) analyses are performed on five liquefaction triggering models, using the field case-history databases from which the respective models were developed. Specifically, for each model, the ROC analyses are used to relate the optimal FS to the ratio of false-positive costs to false-negative costs. This ratio is referred to herein as the cost ratio (CR). In addition, this paper also derives relationships between misprediction costs and optimal PL.

In the following, an overview of the liquefaction triggering models and the associated databases are presented first, which is followed by an overview of the ROC analysis and a demonstration of how it can be used to derive the optimal FS as a function of CR. Next, the optimal FS-CR relationships specific to different liquefaction triggering models, as well as a generic optimal FS-CR relationship, are presented and discussed. Similar relationships are derived for PL from the FS-CR relationships. Finally, a discussion is presented on how the developed relationships can be used in practice.

Data and Methodology

Liquefaction Triggering Models and Associated Databases Used

In this paper, five different liquefaction triggering models based on three different in situ testing methods are analyzed using the field case-history databases from which the respective models were developed. These include the SPT-based models of Boulanger and Idriss (2014) (BI14-SPT) and Cetin et al. (2018) (Cea18-SPT), CPT-based models of Boulanger and Idriss (2014) (BI14-CPT) and Green et al. (2019) (Gea19-CPT), and V_s-based model of Kayen et al. (2013) (Kea13-V_s). Each of these studies present both deterministic and probabilistic variants of the $CRR_{M7.5}$ curve, except for Gea19-CPT, which only presents the former.

Underlying each liquefaction triggering model is the case-history database from which the model was derived. Figs. 1(a–e) contains the probabilistic $CRR_{M7.5}$ curves [except Fig. 1(d) for Gea19-CPT, which only contains their deterministic $CRR_{M7.5}$ curve] and the associated liquefaction case-history data for BI14-SPT, Cea18-SPT, BI14-CPT, Gea19-CPT, and Kea13-V_s. Moreover, Table 2 summarizes the number of "liquefaction," "no liquefaction," and "marginal" cases in the database associated with each model. Note that, in this paper, the "marginal" case histories are treated as "liquefaction" cases. The deterministic $CRR_{M7.5}$ curves recommended by BI14-SPT, BI14-CPT, and Kea13-V_s correspond to a PL of approximately 15%. However, Cea18-SPT recommend their median (i.e., $PL = 50\%$) $CRR_{M7.5}$ curve to be used as their deterministic curve. The deterministic $CRR_{M7.5}$ for each of the preceding models are indicated in Figs. 1(a–e).

ROC analyses were performed on each triggering model using their associated case-history database to relate the optimal FS and PL to the relative costs of mispredicting liquefaction triggering, which is expressed as CR. The following section presents an overview of ROC analysis and how it can be used to derive such relationships.

Overview of ROC Analysis

ROC analysis is a widely adopted tool to evaluate the performance of diagnostic tests. While ROC analysis has seen extensive use in medical diagnostics (e.g., Zou 2007), its use in geotechnical engineering is relatively limited (e.g., Oommen et al. 2010; Maurer et al. 2015a, b, c, 2017a, b, 2019; Green et al. 2015; 2017; Zhu et al. 2017; Upadhyaya et al. 2018, 2019). In particular, in cases where the distribution of "positives" (e.g., liquefaction cases) and "negatives" (e.g., no liquefaction cases) overlap when plotted as a function of diagnostic test results [e.g., FS values; see Fig. 2(a)], ROC analyses can be used to (1) identify the optimum diagnostic threshold (e.g., minimal acceptable FS); and (2) assess the relative efficacy of competing diagnostic models, independent of the thresholds used. A ROC curve is a plot of the True Positive Rate (R_{TP}) (i.e., liquefaction triggered, as predicted) versus the False Positive Rate (R_{FP}) (i.e., liquefaction is predicted to trigger, but did not) for varying threshold values (e.g., minimal acceptable FS). A conceptual illustration of ROC analysis, including the relationship among the distributions for positives and negatives, the threshold value, and the ROC curve, is shown in Fig. 2.

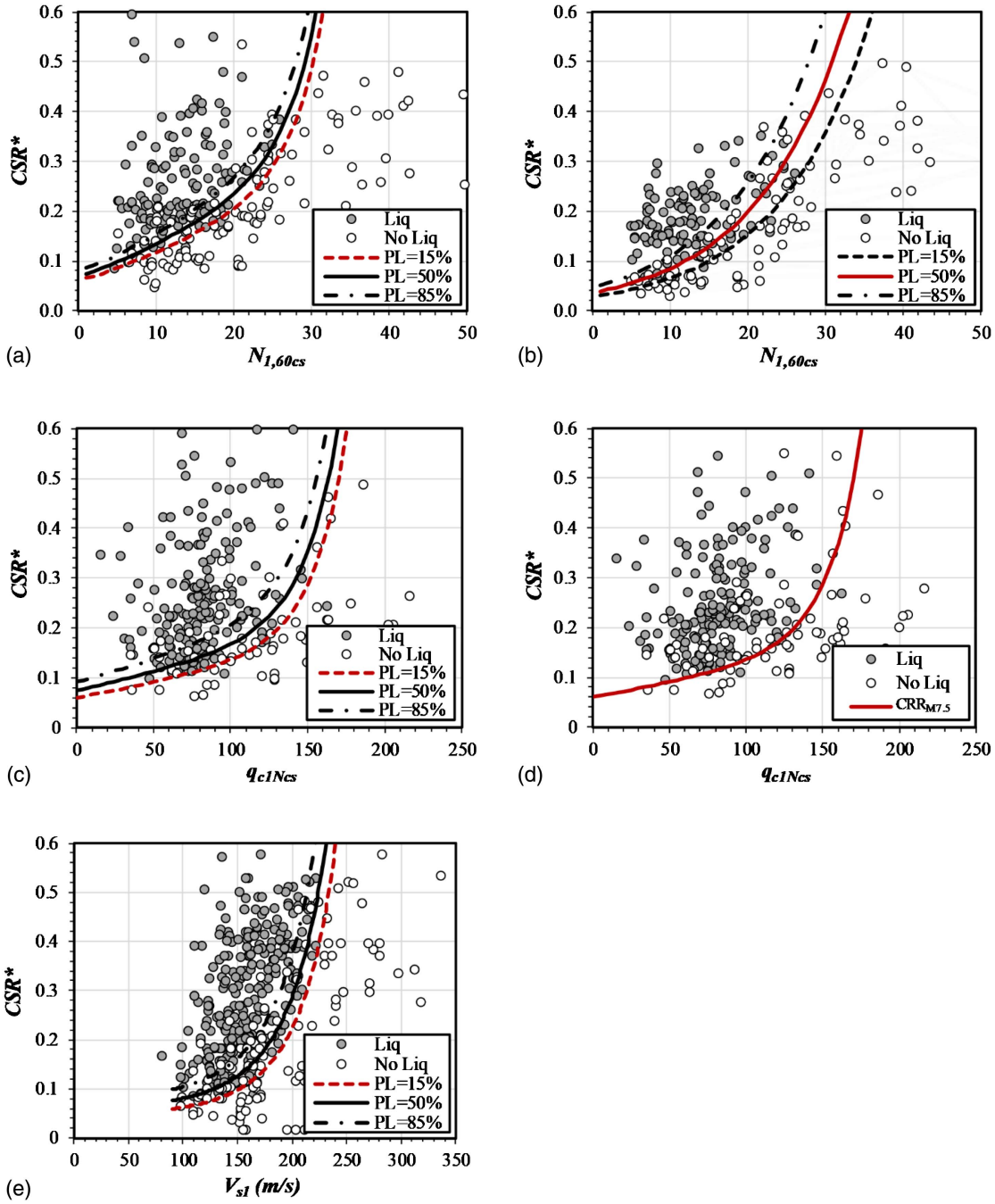

Fig. 1. Case-history data plotted together with the $CRR_{M7.5}$ curves for different probabilities of liquefaction: (a) BI14-SPT; (b) Cea18-SPT; (c) BI14-CPT; (d) Gea19-CPT (deterministic); and (e) Kea13-V_s. The deterministic $CRR_{M7.5}$ curves are shown as the dashed lines in (a), (c), and (e), and as the solid lines in (b) and (d).

Table 2. Summary of number of "liquefaction," "no liquefaction," and "marginal" case histories in the databases used in developing different liquefaction triggering models

Triggering model	Number of cases			
	Liquefaction	No liquefaction	Marginal	Total
BI14-SPT	133	116	3	252
Cea18-SPT	113	95	2	210
BI14-CPT	180	71	2	253
Gea19-CPT	180	71	2	253
Kea13-V_s	287	124	4	415

In ROC space, a diagnostic test that has no predictive ability (i.e., a random guess) results in a ROC curve that plots as 1:1 line through the origin. In contrast, a diagnostic test that has a perfect predictive ability (i.e., a perfect model) plots along the left vertical and upper horizontal axes, connecting at the point (0,1) and indicating the existence of a threshold value that perfectly segregates the data sets (e.g., all cases with liquefaction have FS below this value and all cases without liquefaction have FS above this value). The area under the ROC curve (AUC) is equivalent to the probability that "liquefaction" cases have a lower computed FS than

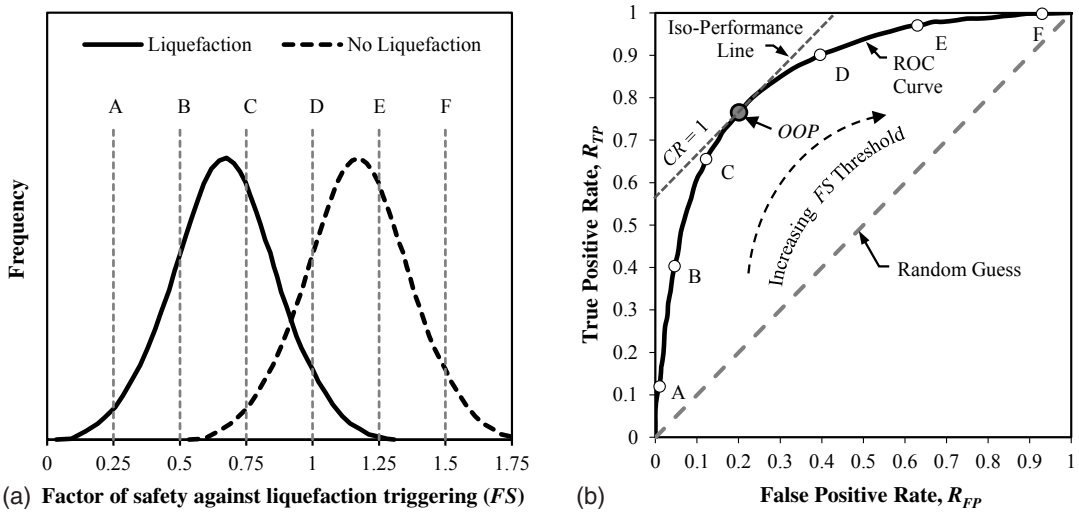

Fig. 2. Conceptual illustration of ROC analyses: (a) frequency distributions of liquefaction and no liquefaction observations as a function of FS; and (b) corresponding ROC curve.

"no liquefaction" cases. As such, higher AUC indicates better predictive capabilities (e.g., Fawcett 2005). To put this into perspective, a random guess returns an AUC of 0.5, whereas a perfect model returns an AUC of 1.

The optimum operating point (OOP) in a ROC analyses is defined as the threshold value (e.g., minimal acceptable FS) that minimizes the misprediction cost, where cost is computed as (Maurer et al. 2015c)

$$cost = C_{FP} \times R_{FP} + C_{FN} \times R_{FN} \tag{2}$$

where C_{FP} and R_{FP} are the cost and rate of false-positive predictions, respectively, and C_{FN} and R_{FN} are the cost and rate of false-negative predictions, respectively. Normalizing Eq. (2) with respect to C_{FN}, and equating R_{FN} to $1 - R_{TP}$, cost may alternatively be expressed as:

$$cost_n = \frac{cost}{C_{FN}} = CR \times R_{FP} + (1 - R_{TP}) \tag{3}$$

where CR is the cost ratio defined as $CR = C_{FP}/C_{FN}$ (i.e., the ratio of the cost of a false-positive prediction to the cost of a false-negative prediction).

As may be surmised, Eq. (3) plots as a straight line in ROC space with a slope of CR and represents a contour of equal performance (i.e., an iso-performance line). Thus, each CR corresponds to a different iso-performance line. One such line, with $CR = 1$ (i.e., false positive costs are equal to false-negative costs) is shown in Fig. 2(b). The point where the iso-performance line is tangent to the ROC curve corresponds to the OOP (e.g., the optimal FS corresponding to a given CR). Thus, by varying the CR values, a relationship between the optimal FS and CR can be developed.

Results and Discussion

Optimal FS versus CR Relationships

ROC analyses were performed on the distributions of FS shown in Fig. 3 for "liquefaction" and "no liquefaction" case histories for each of the five liquefaction triggering models used in this paper (i.e., BI14-SPT, Cea18-SPT, BI14-CPT, Gea19-CPT, and Kea13-V_s). As shown in Fig. 3, lognormal distributions were fit to the "liquefaction" and "no liquefaction" FS histograms for each of the liquefaction triggering models. The expected value (or mean) and standard deviation of the FS's natural logarithm (i.e., $\mu_{\ln FS}$ and $\sigma_{\ln FS}$) for each distribution are listed in Table 3. The ROC curves computed using these distributions are shown in Fig. 4(a). Using each of these ROC curves, optimal values of FS were determined in conjunction with Eq. (3) for CR values ranging from 0.001 to 2. A CR of 0.001 corresponds to a scenario in which the costs of liquefaction are 1,000 times greater than the costs of mitigation (e.g., a critical facility), in which case the minimal acceptable FS should be relatively high. In contrast, a CR of 2 corresponds to a scenario in which the costs of liquefaction are half the costs of mitigation (e.g., an open-air parking lot), in which case the minimal acceptable FS should be relatively low. The relationships between CR and optimal values of FS for BI14-SPT, Cea18-SPT, BI14-CPT, Gea19-CPT, and Kea13-V_s are shown in Fig. 4(b).

As may be observed from Fig. 4(b), the optimal FS is inversely proportional to CR, such that the lower the CR, the higher the optimal FS (i.e., the appropriate degree of conservatism increases). Moreover, the optimal FS-CR relationships are specific to the liquefaction triggering model and associated case-history database. In other words, for a given CR, the optimal FS is specific to the liquefaction triggering model being used. For example, for $CR = 1$, the optimal FS for BI14-SPT, Cea18-SPT, BI14-CPT, Gea19-CPT, and Kea13-V_s are 0.86, 1.13, 0.77, 0.78, and 0.77, respectively [e.g., Fig. 4(b)].

Additionally, the deterministic $CRR_{M7.5}$ curves (i.e., $FS = 1$) for BI14-SPT, Cea18-SPT, BI14-CPT, Gea19-CPT, and Kea13-V_s have associated CR of ~0.47, 1.57, 0.36, 0.33, and 0.36, respectively. This is indicative of the degree of conservatism inherent to the positioning of the deterministic $CRR_{M7.5}$ curve for each model, as well as differences in the range of scenarios represented in the liquefaction case-history databases from which the respective triggering models were derived. As shown, the associated CR for $FS = 1$ are significantly lower than one for BI14-SPT, BI14-CPT, Gea19-CPT, and Kea13-V_s, suggesting that these models implicitly treated the cost of false negatives to be significantly higher than the cost of false positives. On the other hand, the associated CR for $FS = 1$ for Cea18-SPT is greater than one (i.e., $CR = 1.57$ at $FS = 1$), suggesting that Cea18-SPT implicitly assumes that the cost of false negatives to be lower than the cost of false positives. However, because Cea18-SPT recommend their median (i.e., $PL = 50\%$) curve as the deterministic $CRR_{M7.5}$ curve, it might be

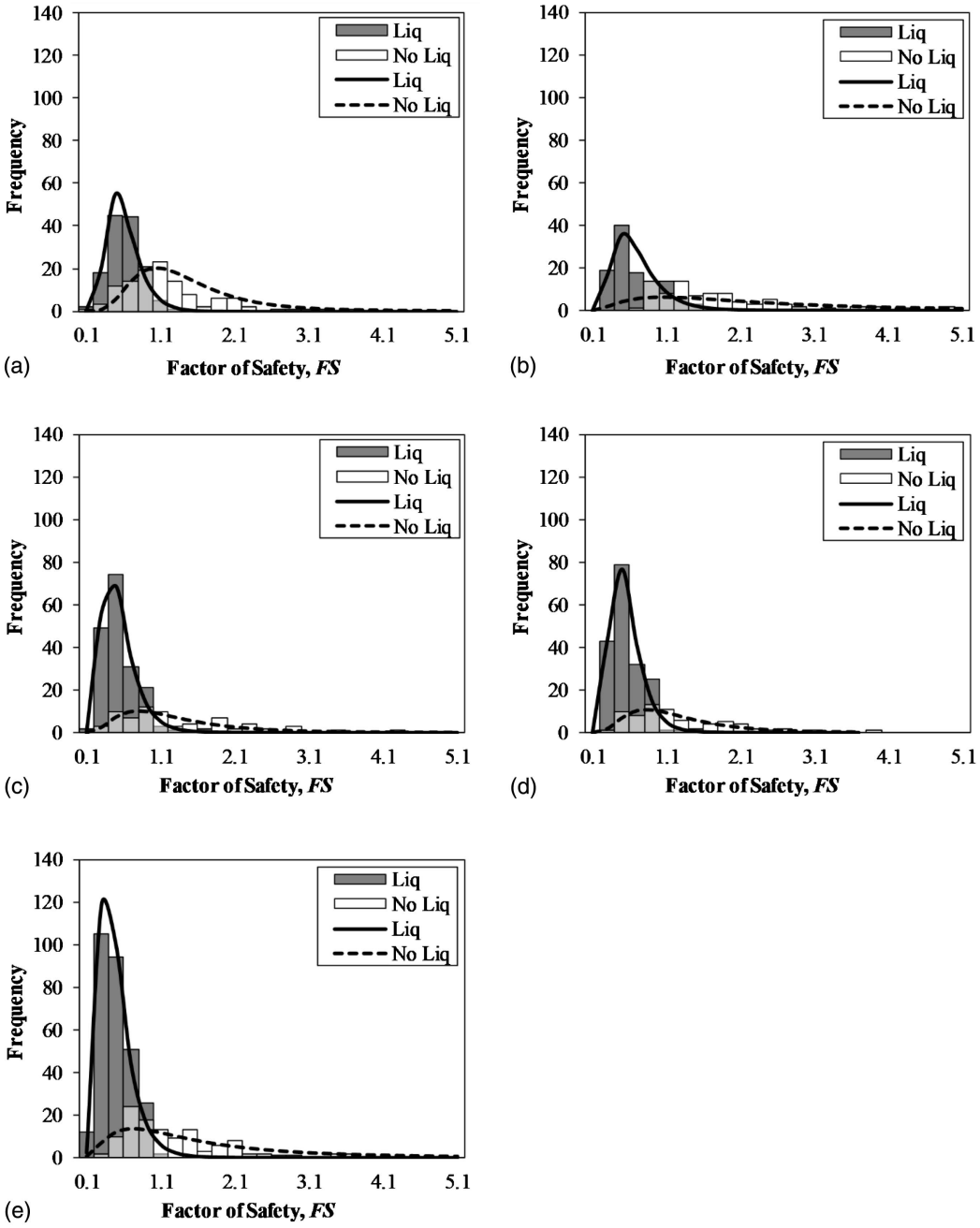

Fig. 3. Distributions of *FS* for the case-history databases used to develop: (a) BI14-SPT; (b) Cea18-SPT; (c) BI14-CPT; (d) Gea19-CPT; and (e) Kea13-V_s. The lighter gray bars indicate the overlapping of the histograms of liquefaction and no liquefaction case histories.

Table 3. Expected value (or mean) and standard deviation of the *FS*'s natural logarithm (i.e., $\mu_{\ln FS}$ and $\sigma_{\ln FS}$) for the "liquefaction" and "no liquefaction" case histories distributions for the databases used in developing the liquefaction triggering models

Triggering model	Liquefaction		No liquefaction	
	$\mu_{\ln FS}$	$\sigma_{\ln FS}$	$\mu_{\ln FS}$	$\sigma_{\ln FS}$
BI14-SPT	−0.548	0.364	0.259	0.457
Cea18-SPT	−0.456	0.443	0.712	0.813
BI14-CPT	−0.701	0.422	0.116	0.584
Gea19-CPT	−0.647	0.377	0.098	0.536
Kea13-V_s	−0.817	0.451	0.259	0.764
Combined	−0.706	0.425	0.203	0.610

expected that CR ≈ 1 for FS = 1 (i.e., the cost of false negatives and false positives are approximately equal). The reason this is not the case is due to the limited number of case histories in the case-history database and the way sampling bias was accounted for by Cetin et al. (2018) in regressing their $CRR_{M7.5}$ curves (i.e., the way the overrepresentation of liquefaction case histories versus no liquefaction case histories in the database, as compared to the true distribution of these cases in a region impacted by an earthquake, is accounted for).

As discussed in the Introduction, the choice of the optimal *FS* for any engineering project should be guided by the associated costs (or consequences) of mispredicting liquefaction. As such, the optimal *FS-CR* relationships derived herein can be used to

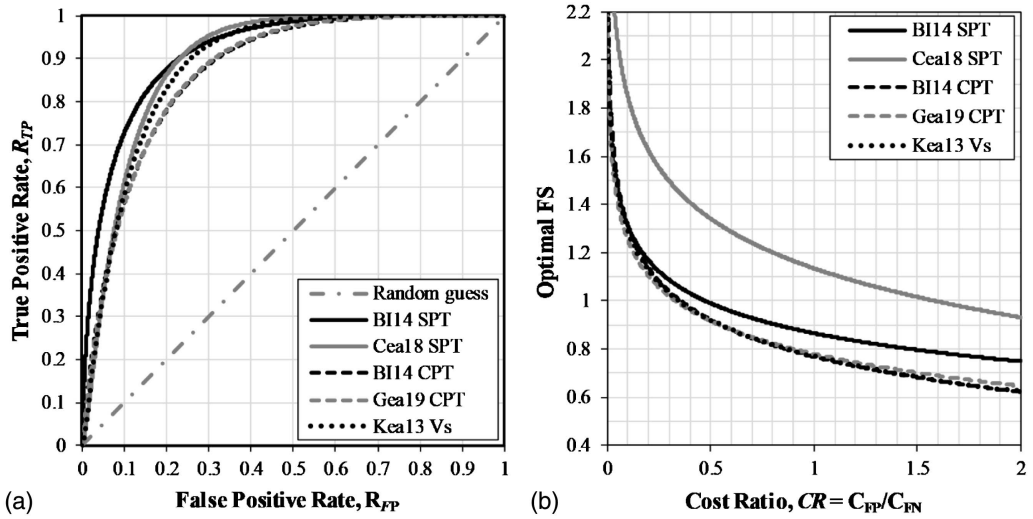

Fig. 4. ROC analyses of *FS* data for BI14-SPT, Cea18-SPT, BI14-CPT, Gea19-CPT, and Kea13-V_s: (a) ROC curves; and (b) optimal *FS* versus *CR* curves.

determine triggering model-specific optimal *FS* for a project. However, selecting a value for *FS* for a project that depends on the triggering model being used will likely cause confusion, despite a general understanding of the assumptions inherent to each triggering model having different associated levels of conservatisms. Accordingly, the *FS* data for the triggering models were combined, with the exception of the data for Cea18-SPT, and an optimal *FS-CR* relationship was derived for this combined case-history database. The reason that the Cea18-SPT case-history data was excluded is because their deterministic $CRR_{M7.5}$ corresponds to $PL = 50\%$ (i.e., median $CRR_{M7.5}$ curve), as opposed to $PL \approx 15\%$ used by the other models.

Fig. 5(a) shows the ROC curve for the combined *FS* case-history data and Fig. 5(b) shows the corresponding optimal *FS-CR* curve. By combining the *FS* data from different models, the degree of conservatism inherent to the associated deterministic $CRR_{M7.5}$ curves is "averaged out." Although this averaging is being "forced" by the authors by using the combined case-history data set, the need for this will be negated as the consistency in the case-history databases for each of the triggering model increases (e.g., number of liquefaction and no liquefaction cases, interpretation of the case histories, etc.) and the consistency in how the $CRR_{M7.5}$ curves are regressed converges. As a result, the use of the generic *FS-CR* curve is preferred by the authors for forward analyses over the model-specific *FS-CR* curves.

Optimal PL versus CR Relationships

For each of the liquefaction triggering models used in this paper that have probabilistic variants, there is a one-to-one relationship between *FS* and *PL* (i.e., each *FS* corresponds to a certain *PL*), shown in Fig. 6(a), which is a result of the constraints imposed on the regression analyses used to develop the probabilistic $CRR_{M7.5}$ curves. Accordingly, the *FS-PL* relationships shown in Fig. 6(a)

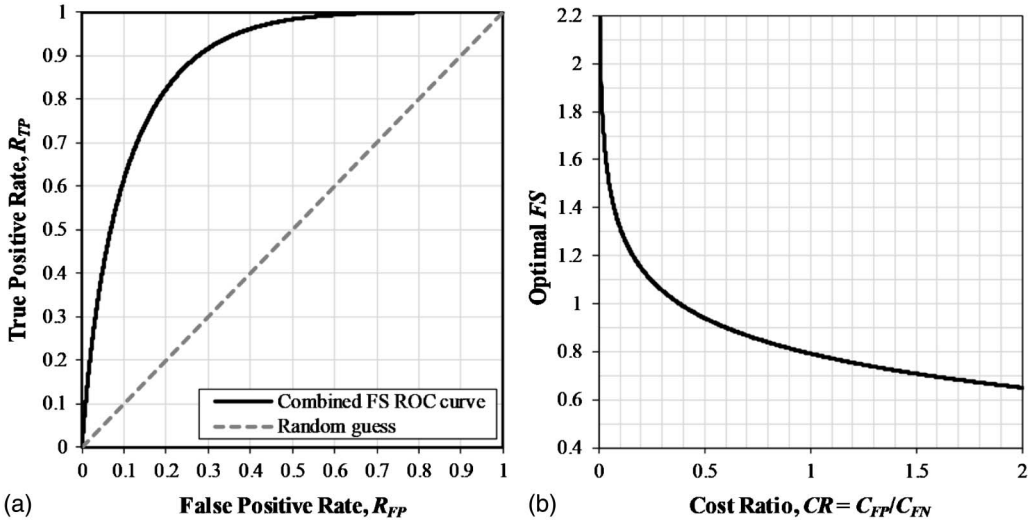

Fig. 5. ROC analyses of *FS* data combined from BI14-SPT, BI14-CPT, Gea19-CPT, and Kea13-V_s: (a) ROC curve; and (b) optimal *FS* versus *CR* curves.

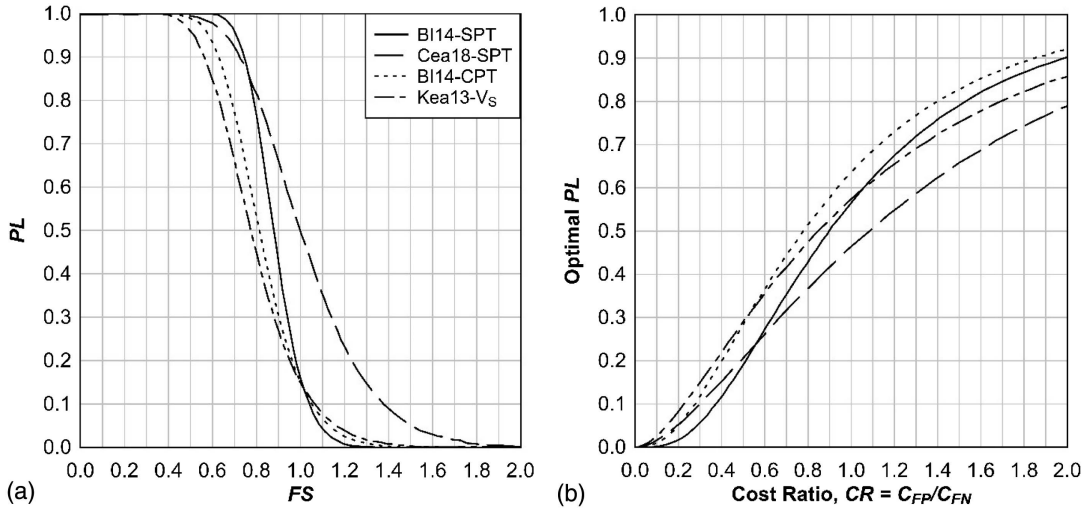

Fig. 6. (a) *PL-FS* curves for the triggering models; and (b) optimal *PL-CR* curves computed using the *PL-FS* curves and the optimal *FS-CR* curves.

can be used in conjunction with the *FS-CR* curves shown in Fig. 4(b) to compute *PL-CR* curves. The resulting *PL-CR* curves for BI14-SPT, Cea18-SPT, BI14-CPT, and Kea13-V_s triggering models are shown in Fig. 6(b).

As may be observed from Fig. 6(b), the optimal *PL* is directly proportional to *CR* such that as *CR* increases, the corresponding optimal *PL* increases. As with the optimal *FS-CR* curves, the optimal *PL-CR* curves are also specific to the probabilistic liquefaction triggering models and the respective databases used in deriving them. Accordingly, a "generic" optimal *PL-CR* curve is also derived. Toward this end, a weighted average of the *FS-PL* relationships shown in Fig. 6(a) is used in conjunction with the generic *FS-CR* curve shown in Fig. 5(b) to compute a generic *PL-CR* curve, shown in Fig. 7. The generic *PL-CR* curve would be used similarly as the generic *FS-CR* curve.

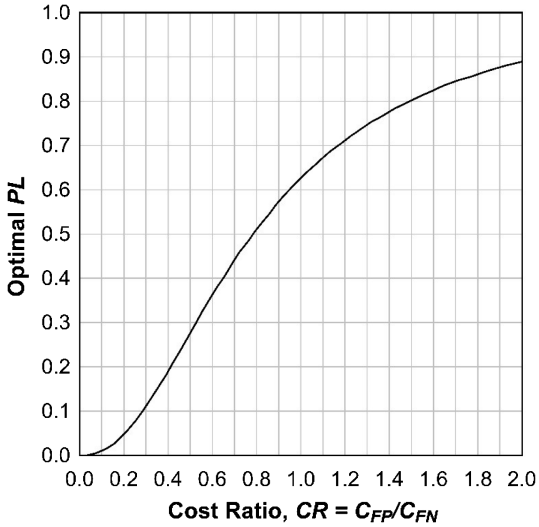

Fig. 7. Optimal *PL* versus *CR* curve for combined triggering models, computed by using an average of the *PL-FS* relationships for the triggering models shown in Fig. 6(a) and the combined data optimal FS-CR curve shown in Fig. 5(b).

Using the Optimal FS/PL versus CR Relationships in Forward Analyses

To facilitate use of the optimal *FS-CR* curves shown in Figs. 4(b) and 5(b), a simple equation for the curves is provided

$$Optimal\,FS = c_1 \cdot CR^{c_2} + c_3 \tag{4}$$

where c_1, c_2, and c_3 = regression coefficients and are listed in Table 4 for each of the triggering models and the combined model. Similarly, a simple equation for the optimal *PL-CR* curves shown in Figs. 6(b) and 7(b) is provided

$$Optimal\,PL = d_1 + d_2 \cdot CR + d_3 \cdot CR^2 + d_4 \cdot CR^3 + d_5 \cdot CR^4 + d_6 \cdot CR^5 \tag{5}$$

where d_1, d_2, d_3, d_4, d_5, and d_6 = regression coefficients and are also listed in Table 4 for each of the probabilistic triggering models and the combined model.

To illustrate how an optimal *FS-CR* curve can be used to select an optimal *FS* for a project based on cost considerations, the following simple example is presented using the generic optimal *FS-CR* curve shown in Fig. 5(b). First, consider a site that has a computed *FS* of 1 for a design earthquake scenario. If a one-story residential building is to be built at this site, for which the *CR* is estimated as 0.7, using Fig. 5(b), the optimal *FS* threshold for decision making would be 0.87. Since the computed *FS* is greater than the optimal *FS* for this scenario, it is more economical to leave the site unimproved and pay for the cost of repairs due to damages from liquefaction, if it occurs (note that liquefaction triggering and lateral spreading generally does not pose a risk to life or safety, e.g., Green and Bommer 2019). On the other hand, if an essential facility (e.g., a hospital building) is to be built at the site and has an estimated *CR* of 0.05, using Fig. 5(b) the optimal *FS* decision threshold would be 1.49. In this case, the computed *FS* is lower than the optimal *FS* and thus performing ground improvement upfront is favorable.

The optimal *PL-CR* curves are used in a similar manner as the optimal *FS-CR* curves (i.e., the predicted *PL* at a site without any liquefaction mitigation can be compared with the optimal *PL* at the *CR* of interest to determine whether or not liquefaction mitigation is worth the expense). It should be noted, however, that for each of the

Table 4. Regression coefficients for simple models for optimal *FS-CR* curves and optimal *PL-CR* curves

Triggering model	Regression coefficients								
	c_1	c_2	c_3	d_1	d_2	d_3	d_4	d_5	d_6
BI14-SPT	1.831	−0.095	−0.969	0.011040	−0.3857	2.368	−2.088	0.7640	−0.104
Cea18-SPT	8.894	−0.033	−7.762	−0.003392	0.1884	1.021	−1.049	0.4507	−0.0735
BI14-CPT	4.846	−0.045	−4.081	−0.001100	−0.1047	2.353	−2.542	1.1140	−0.1803
Gea19-CPT	4.084	−0.048	−3.308	—	—	—	—	—	—
Kea13-V_s	4.846	−0.045	−4.081	−0.007239	0.2654	1.238	−1.505	0.7051	−0.1207
Combined	2.345	−0.087	−1.553	0.002455	−0.1860	2.594	−2.829	1.2500	−0.2028

liquefaction triggering models used in this paper, there is a one-to-one relationship between *FS* and *PL* (i.e., each *FS* corresponds to a certain *PL*), which is a result of the constraints imposed on the regression analyses used to develop the probabilistic $CRR_{M7.5}$ curves. Therefore, the optimal $FS - CR$ curves and optimal $PL - CR$ curves contain similar information. Also, in current practice, where the $CRR_{M7.5}$ curve for a selected value of *PL* is used in design in the same manner as a deterministic liquefaction triggering curve, there is no additional benefit from using *PL*, in lieu of *FS*, as your decision metric. In this same vein, it is important to note that the probabilistic liquefaction models considered herein postulate a conditional probability of liquefaction (i.e., *PL* given a value of CSR^*). Alternatively, a risk-based approach can be used to obtain an absolute value of the probability of liquefaction (e.g., Kramer and Mayfield 2007; Green et al. 2020). However, these approaches require a degree of sophistication, including additional input parameters that are beyond those commonly used in current practice, and thus are outside the scope of this paper.

Finally, in the simple preceding example, the *CR* are simply stated without explanation, although in general it would be expected that an essential facility would have a lower *CR* than a non-essential facility. However, it can be foreseen that the selection of the *CR* for a project may require broader consideration than direct and indirect costs related to just that project alone. Recall that the *CR* is the ratio of costs associated with false-positive predictions to the costs associated with false-negative predictions. Examples of direct and indirect costs of false-positive predictions include, for example, the costs associated with ground improvement, increased time to completion of the project due to implementation of ground improvement, and more robust foundation design and construction. Examples of the direct and indirect costs of false-negative predictions could include the costs associated with property damage, reconstruction and rehabilitation costs, and temporary housing costs during reconstruction. Accordingly, broader-scale issues may also need to be considered in estimating these costs. For example, the cost of temporarily housing families while repairs are being made to their single-family houses damaged by liquefaction does not necessarily scale linearly with the cost associated with just one house and family. The reason for this is that temporary housing facilities may be overwhelmed by the large demand if the residents in several large subdivisions need temporary housing at the same time. The same is true for the cost of repairing multiple single-family houses, where the demand for building supplies and skilled tradesmen may exceed the available capacity. As a result, it is envisioned that the *CR* for a specific project would be determined both by design engineers for the project and building regulators, with the latter being more attuned to broader considerations. In line with this, considerations of life-cycle costs (e.g., the response of an infrastructure asset to earthquake motions having a range of return periods) and limitations in the efficacy of selected ground improvement techniques to mitigate damage could be considered in estimating *CR*. Clearly, the adoption of the proposed framework will shift discussions/debates about what optimal *FS* or *PL* should be used for a project to what *CR* is most appropriate for a project. This is more in line with a risk-type philosophy than arguing for a higher or lower minimal acceptable *FS* based on heuristic-based rules of thumb.

Summary and Concluding Remarks

This paper demonstrates how costs of mispredicting liquefaction triggering can be utilized in selecting an appropriate minimal acceptable *FS* against liquefaction (i.e., "optimal" *FS*) for a project. Specifically, relationships between the optimal *FS* and the ratio of false-positive prediction costs to false-negative prediction costs (i.e., *CR*) were derived by performing ROC analyses on five different liquefaction triggering models (i.e., BI14-SPT, Cea18-SPT, BI14-SPT, Gea19-CPT, and Kea13-V_s), in conjunction with their respective case-history databases. The optimal *FS-CR* relationships were found to be specific to the liquefaction triggering models and associated case-history databases. This is indicative of the assumptions inherent to each triggering model having different associated levels of conservatisms, as well as differences in the range of scenarios represented in the liquefaction case-history databases from which the respective triggering models were derived. Consequently, a "generic" optimal *FS-CR* was derived by combining *FS* data from the specific models, which "averages out" the degree of conservatism inherent to the associated deterministic $CRR_{M7.5}$ curves for the different models. It is noted, however, that the need for using combined liquefaction case-history data sets will be negated as the consistency in the case-history databases for each of the triggering models, and how the $CRR_{M7.5}$ curves are regressed increases. For now, the use of the generic *FS-CR* curve is preferred by the authors for forward analyses over the model-specific *FS-CR* curves.

Using *PL* as an alternative to *FS*, relationships between *CR* and the optimal *PL* were also derived using *FS-PL* relationships in conjunction with the optimal *FS-CR* curves. The optimal *PL-CR* curves, however, do not provide any additional information over the optimal *FS-CR* curves. This is because there is a direct correlation between *FS* and *PL* due to the way the probabilistic triggering models are currently developed.

The costs associated with false-positive and false-negative predictions that are used to compute *CR* may require broader consideration than just the direct and indirect costs related to the project at hand. The reason for this is these costs do not necessarily scale linearly with the amount of infrastructure impacted. As a result, it is envisioned that the *CR* for a specific project would be determined both by design engineers for the project and building regulators, with the latter being more attuned to broader considerations. In line with this, considerations of life-cycle costs (e.g., the response of an infrastructure asset to earthquake motions having a

range of return periods) and limitations in the efficacy of selected ground improvement techniques to mitigate damage can be considered in estimating CR.

Finally, the proposed relationships correlate FS and PL to CR because FS, and less so PL, are common regulatory building requirements. However, FS and PL only represent conditions at a specific location and depth at a site and do not necessarily reflect liquefaction damage potential, which is more of a function of the liquefaction response of the entire soil profile. As a result, correlations relating liquefaction damage potential indices, such as LPI, LSN, and LPI_{ish} (Iwasaki et al. 1978; van Ballegooy et al. 2014; Maurer et al. 2015d), to CR would seemingly be more appropriate than optimal FS/PL-CR correlations. In this vein, the framework proposed herein to develop the optimal FS/PL-CR correlations could be readily used to develop optimal LPI_{ish}-CR correlations, for example. However, this would require buy-in from regulators and building code officials in adopting LPI_{ish}, for example, in lieu of FS as a design/performance metric.

Data Availability Statement

Some or all data, models, or code that support the findings of this paper are available from the corresponding author upon reasonable request.

Acknowledgments

The authors greatly acknowledge the funding support through the National Science Foundation (NSF) Grant Nos. CMMI-1435494, CMMI-1751216, CMMI-1825189, and CMMI-1937984, as well as Pacific Earthquake Engineering Research Center (PEER) Grant No. 1132-NCTRBM and U.S. Geological Survey (USGS) Award No. G18AP-00006. However, any opinions, findings, and conclusions or recommendations expressed in this paper are those of the authors and do not necessarily reflect the views of NSF, PEER, or USGS.

References

Boulanger, R. W., and I. M. Idriss. 2012. "Probabilistic standard penetration test-based liquefaction-triggering procedure." *J. Geotech. Geoenviron. Eng.* 138 (10): 1185–1195. https://doi.org/10.1061/(ASCE)GT.1943-5606.0000700.

Boulanger, R. W., and I. M. Idriss. 2014. *CPT and SPT based liquefaction triggering procedures*. Rep. No. UCD/CGM-14/01. Davis, CA: Center for Geotechnical Modelling.

BSSC (Building Seismic Safety Council). 2009. *NEHRP recommended seismic provisions for new buildings and other structures (FEMA P-750)*. Washington, DC: Federal Emergency Management Agency.

Cetin, K. O., R. B. Seed, A. Der Kiureghian, K. Tokimatsu, L. F. R. E. HarderKayen, R. Kayen, and R. E. S. Moss. 2004. "Standard penetration test-based probabilistic and deterministic assessment of seismic soil liquefaction potential." *J. Geotech. Geoenviron. Eng.* 130 (12): 1314–1340. https://doi.org/10.1061/(ASCE)1090-0241(2004)130:12(1314).

Cetin, K. O., R. B. Seed, R. E. Kayen, R. E. S. Moss, H. T. Bilge, M. Ilgac, and K. Chowdhury. 2018. "SPT-based probabilistic and deterministic assessment of seismic soil liquefaction triggering hazard." *Soil Dyn. Earthquake Eng.* 115 (Dec): 698–709. https://doi.org/10.1016/j.soildyn.2018.09.012.

Fawcett, T. 2005. "An introduction to ROC analysis." *Pattern Recognit. Lett.* 27 (8): 861–874. https://doi.org/10.1016/j.patrec.2005.10.010.

Green, R. A., et al. 2020. "Liquefaction hazard in the groningen region of the Netherlands due to induced seismicity." *J. Geotech. Geoenviron. Eng.* 146 (8): 04020068. https://doi.org/10.1061/(ASCE)GT.1943-5606.0002286.

Green, R. A., and J. J. Bommer. 2019. "What is the smallest earthquake magnitude that needs to be considered in assessing liquefaction hazard?" *Earthquake Spectra* 35 (3): 1441–1464. https://doi.org/10.1193/032218EQS064M.

Green, R. A., J. J. Bommer, A. Rodriguez-Marek, B. W. Maurer, P. Stafford, B. Edwards, P. P. Kruiver, G. de Lange, and J. van Elk. 2019. "Addressing limitations in existing 'simplified' liquefaction triggering evaluation procedures: Application to induced seismicity in the Groningen gas field." *Bull. Earthquake Eng.* 17 (3): 4539–4557. https://doi.org/10.1007/s10518-018-0489-3.

Green, R. A., B. W. Maurer, M. Cubrinovski, and B. A. Bradley. 2015. "Assessment of the relative predictive capabilities of CPT-based liquefaction evaluation procedures: Lessons learned from the 2010–2011 Canterbury earthquake sequence." In *Proc., 6th Int. Conf. on Earthquake Geotechnical Engineering*. London: International Society for Soil Mechanics and Geotechnical Engineering.

Green, R. A., B. W. Maurer, and S. van Ballegooy. 2018. "The influence of the non-liquefied crust on the severity of surficial liquefaction manifestations: Case history from the 2016 valentine's day earthquake in New Zealand." In *Proc., Geotechnical Earthquake Engineering and Soil Dynamics V (GEESD V)*, 21–32. Reston, VA: ASCE.

Green, R. A., S. Upadhyaya, C. M. Wood, B. W. Maurer, B. R. Cox, L. Wotherspoon, B. A. Bradley, and M. Cubrinovski. 2017. "Relative efficacy of CPT- versus Vs-based simplified liquefaction evaluation procedures." In *Proc., 19th Int. Conf. on Soil Mechanics and Geotechnical Engineering*. London: International Society for Soil Mechanics and Geotechnical Engineering.

Idriss, I. M., and R. W. Boulanger. 2008. *Soil liquefaction during earthquakes*. Oakland, CA: Earthquake Engineering Research Institute.

Idriss, I. M., and R. W. Boulanger. 2010. *SPT-based liquefaction triggering procedures*. Rep. UCD/CGM-10/02. Davis, CA: Univ. of California at Davis.

Iwasaki, T., F. Tatsuoka, K. Tokida, and S. Yasuda. 1978. "A practical method for assessing soil liquefaction potential based on case studies at various sites in Japan." In *Proc., 2nd Int. Conf. on Microzonation*. Reston, VA: ASCE.

Kayen, R., R. Moss, E. Thompson, R. Seed, K. Cetin, A. Kiureghian, Y. Tanaka, and K. Tokimatsu. 2013. "Shear-wave velocity–based probabilistic and deterministic assessment of seismic soil liquefaction potential." *J. Geotech. Geoenviron. Eng.* 139 (3): 407–419. https://doi.org/10.1061/(ASCE)GT.1943-5606.0000743.

Kramer, S. L., and R. T. Mayfield. 2007. "Return period of soil liquefaction." *J. Geotech. Geoenviron. Eng.* 133 (7): 802–813. https://doi.org/10.1061/(ASCE)1090-0241(2007)133:7(802).

Martin, G. R., and M. Lew. 1999. *Recommended procedures for implementation of DMG Special Publication 117 guidelines for analysing and mitigating liquefaction in California*. Los Angeles: Univ. of Southern California.

Maurer, B. W., R. A. Green, M. Cubrinovski, and B. Bradley. 2015a. "Fines-content effects on liquefaction hazard evaluation for infrastructure during the 2010–2011 Canterbury, New Zealand earthquake sequence." *Soil Dyn. Earthquake Eng.* 76 (Sep): 58–68. https://doi.org/10.1016/j.soildyn.2014.10.028.

Maurer, B. W., R. A. Green, M. Cubrinovski, and B. Bradley. 2015b. "Assessment of CPT-based methods for liquefaction evaluation in a liquefaction potential index framework." *Géotechnique* 65 (5): 328–336. https://doi.org/10.1680/geot.SIP.15.P.007.

Maurer, B. W., R. A. Green, M. Cubrinovski, and B. Bradley. 2015c. "Calibrating the liquefaction severity number (LSN) for varying misprediction economies: A case study in Christchurch, New Zealand." In *Proc., 6th Int. Conf. on Earthquake Geotechnical Engineering*. London: International Society for Soil Mechanics and Geotechnical Engineering.

Maurer, B. W., R. A. Green, and O.-D. S. Taylor. 2015d. "Moving towards an improved index for assessing liquefaction hazard: Lessons from historical data." *Soils Found.* 55 (4): 778–787.

Maurer, B. W., R. A. Green, S. van Ballegooy, B. A. Bradley, and S. Upadhyaya. 2017a. *Performance comparison of probabilistic and*

deterministic liquefaction triggering models for hazard assessment in 23 global earthquakes, 31–42. Reston, VA: ASCE.

Maurer, B. W., R. A. Green, S. van Ballegooy, and L. Wotherspoon. 2017b. "Assessing liquefaction susceptibility using the CPT soil behavior type index." In *Proc., 3rd Int. Conf. on Performance-Based Design in Earthquake Geotechnical Engineering*. London: International Society for Soil Mechanics and Geotechnical Engineering.

Maurer, B. W., R. A. Green, S. van Ballegooy, and L. Wotherspoon. 2019. "Development of region-specific soil behavior type index correlations for evaluating liquefaction hazard in Christchurch, New Zealand." *Soil Dyn. Earthq. Eng.* 117 (4): 96–105. https://doi.org/10.1016/j.soildyn.2018.04.059.

Moss, R. E. S., R. B. Seed, R. E. Kayen, J. P. Stewart, A. Der Kiureghian, and K. O. Cetin. 2006. "CPT-based probabilistic and deterministic assessment of in situ seismic soil liquefaction potential." *J. Geotech. Geoenviron. Eng.* 132 (8): 1032–1051. https://doi.org/10.1061/(ASCE)1090-0241(2006)132:8(1032).

Oommen, T., L. G. Baise, and R. Vogel. 2010. "Validation and application of empirical liquefaction models." *J. Geotech. Geoenviron. Eng.* 136 (12): 1618–1633. https://doi.org/10.1061/(ASCE)GT.1943-5606.0000395.

Robertson, P. K., and C. E. Wride. 1998. "Evaluating cyclic liquefaction potential using cone penetration test." *Can. Geotech. J.* 35 (3): 442–459. https://doi.org/10.1139/t98-017.

Seed, H. B., and I. M. Idriss. 1971. "Simplified procedure for evaluating soil liquefaction potential." *J. Soil Mech. Found. Div.* 97 (9): 1249–1273.

Upadhyaya, S., R. A. Green, B. W. Maurer, and A. Rodriguez-Marek. 2019. "Selecting factor of safety against liquefaction for design based on cost considerations." In *Proc., 7th Int. Conf. on Earthquake Geotechnical Engineering*. London: International Society for Soil Mechanics and Geotechnical Engineering.

Upadhyaya, S., B. W. Maurer, R. A. Green, and A. Rodriguez-Marek. 2018. *Effect of non-liquefiable high fines-content, high plasticity soils on liquefaction potential index (LPI) performance*, 191–198. Reston, VA: ASCE.

van Ballegooy, S., P. Malan, V. Lacrosse, M. E. Jacka, M. Cubrinovski, J. D. Bray, T. D. O'Rourke, S. A. Crawford, and H. Cowan. 2014. "Assessment of liquefaction-induced land damage for residential Christchurch." *Earthquake Spectra* 30 (1): 31–55. https://doi.org/10.1193/031813EQS070M.

Whitman, R. V. 1971. "Resistance of soil to liquefaction and settlement." *Soils Found.* 11 (4): 59–68. https://doi.org/10.3208/sandf1960.11.4_59.

Zhu, J., L. G. Baise, and E. M. Thompson. 2017. "An updated geospatial liquefaction model for global application." *Bull. Seismol. Soc. Am.* 107 (3): 1365–1385. https://doi.org/10.1785/0120160198.

Zou, K. H. 2007. "Receiver operating characteristic (ROC) literature research." Accessed March 10, 2016. http://www.spl.harvard.edu/archive/spl-pre2007/pages/ppl/zou/roc.html.